Colloid Polym Sci (2008) 286:621–629
DOI 10.1007/s00396-007-1808-4

ORIGINAL CONTRIBUTION

Drying dissipative patterns of colloidal crystals of silica spheres on a cover glass at the regulated temperature and humidity

Tsuneo Okubo · Keisuke Kimura · Akira Tsuchida

Received: 30 August 2007 / Revised: 11 October 2007 / Accepted: 17 November 2007 / Published online: 11 December 2007

Abstract Influences of temperature and humidity on the drying dissipative patterns of colloidal crystals of silica spheres (103 nm in diameter) were studied. The broad ring pattern, which is one of the typical macroscopic drying structures, became sharp as temperature rose and/or humidity decreased. Furthermore, number of the spoke-like cracks decreased as temperature and/or humidity increased. The water evaporation from a liquid surface to air and the convectional flow of water and colloidal spheres were important for the macroscopic pattern formation.

Keywords Drying pattern · Dissipative structure · Temperature · Humidity · Colloidal crystal · Colloidal silica spheres

Introduction

To understand the mechanisms of the dissipative structure formation in nature, the convectional, sedimentation, and drying dissipative patterns have been studied in our laboratory. Many kinds of the suspensions of colloidal silica spheres and anisotropic-shaped colloidal particles, as well as of the solutions of simple and poly-electrolytes, detergents, dyes, biopolymers, and water-soluble neutral polymers were dried on a cover glass, as well as a glass dish and/or a watch glass. Table 1 compiles the macroscopic and microscopic patterns observed hitherto [1–27]. Interestingly, macroscopic broad ring patterns of the hill accumulated with solutes in the outside edges were formed for almost all solutes. For the nonspherical solutes, a central round hill was formed in the central area in addition to the broad rings. Macroscopic spoke-like cracks or fine hills, including flickering spoke-like ones, were also observed for many solutes. The convection of water and the solutes at different rates under gravity and the translational and rotational Brownian movement of the latter were important for the macroscopic pattern formation. Furthermore, so many types of patterns such as branch-like, arc-like, block-like, star-like, cross-like, and string-like ones were observed in the microscopic scale. These microscopic drying patterns were reflected from the shape, size, and flexibility of the solutes themselves. In addition, it has been supported that, in the microscopic pattern formation, the electrostatic and hydrophobic interactions between solutes molecules or particles and/or the solute and substrate in the course of solidification are of importance. One of the important findings in our experiments was that the vague primitive patterns already formed in the suspension state before dryness, and they grew toward the structures during the course of solidification. The authors believe that the solute information (property) such as shape, size, hydrophobicity, hydrophilicity, and hydrophile–liophile balance characters of solutes are transmitted, amplified, and selected toward the final process of drying patterns through the convectional flow, sedimentation, and flow birefringence of solutes under earth gravity (e.g., see [28, 29]). Thus, studies on the dissipative patterns during the course of dryness are very important for the understanding of the self-organization processes in nature. It should be mentioned in

T. Okubo (✉)
Institute for Colloidal Organization,
Hatoyama 3-1-112,
Uji, Kyoto 611-0012, Japan
e-mail: okubotsu@ybb.ne.jp

T. Okubo
Cooperative Research Center, Yamagata University,
Johnan 4-3-16,
Yonezawa 992-8510, Japan

K. Kimura · A. Tsuchida
Department of Applied Chemistry, Gifu University,
Yanagido 1-1,
Gifu 501-1193, Japan

Table 1 Dissipative patterns observed during the course of drying suspensions and solutions

Drying patterns				
Macroscopic	Broad ring	Normal BR	Single BR	[1–16, 18–21, 25, 27]
			Multiple BR	[3, 8, 10, 14, 15, 18]
			Square broad band	[17]
		Notched BR		[1, 2, 21]
		Inner and outer BR		[18, 20, 27]
		Multiple fine circles		[5]
	Spoke lines	Spoke crack		[1, 2, 6, 16, 18]
		Spoke hill	Normal SH	[5]
			Flickering SH	[15]
	Ring	Ring crack		[1, 2, 10]
	Wave			[6, 10, 19, 25, 27]
	Column			[17]
	Central round hill			[7, 9, 10, 15]
	Layers			[27]
Microscopic	Spoke line	Spoke crack		[1, 2, 13, 15, 16, 19, 20, 25]
	Multiple ring	MR crack		[13, 15, 19, 25]
	Branch			[1, 4, 6–9]
	Earthworm			[2]
	String			[3, 8, 9, 12]
	Dendrite, leaf			[11, 19, 25]
	Star			[3, 7–9, 11, 19, 25]
	Street road			[3, 8, 21]
	Flower			[3, 4, 15, 18, 21]
	Block	Normal B		[7–9,14,15,18]
		"Shigaraki Yaki"		[5]
	Cross			[4, 10, 18]
	Rod			[18]
	Arc			[4]
	Needle			[21]
	Wrinkled			[7, 10]
	Chapped			[7, 10]
	Netting			[6]
Sedimentation pattern				
Macroscopic	Broad ring			[11–14, 19, 25]
Microscopic	Vague wrinkled			[7]
Convectional pattern				
Macroscopic	Spoke line			[5, 22–24]
	Hexagonal circulating cell (Bernard cell)			[26]
	Cyclic circulating cell			[5]
	Smoke			[5]
	Cooperative circulation			[13]
Microscopic	Cell convection (Terada cell)			[5, 22–24]

this paper that several papers on the drying pattern formation of colloidal suspensions and solutions have already been reported by other distinguished researchers [30–43].

Most of our experiments on the dissipative patterns have been made at a constant temperature but at unregulated humidity of air. Temperature and humidity are essentially important factors for the pattern formation through the evaporation of water at the liquid–air interface and resulting convectional flow of solutes and solvent. To understand the contributions of air temperature and humidity clearly, the drying patterns were observed at the regulated temperature and humidity in this work.

Experimental

Materials

CS82 silica spheres were kindly donated from Catalysts & Chemicals Ind. (Tokyo). Diameter, standard deviation from

the mean diameter, and polydispersity index of the spheres were 103, 13.2, and 0.128 nm, respectively. These size parameters were determined on an electron microscope (transmission electron microscopy, Hitachi, H8100) in our laboratory. The charge density of the spheres was determined by conductometric titration with a Horiba conductivity meter, model DS-14 (Kyoto). Strongly acidic charge density was 0.38 μC/cm^2. The spheres were carefully purified several times using an ultrafiltration cell (model 202, membrane: Diaflo-XM300, Amicon). Then, the stock sample suspension was treated on a mixed bed of cation- and anion-exchange resins [Bio-Rad, AG501-X8(D), 20–50 mesh] for more than 10 years before use. The stock suspension, thus, obtained was colloidal crystal and emitted very strong iridescent blue colors. Water used for the sample preparation was purified by a Milli-Q reagent grade system (Milli-RO5 plus and Milli-Q plus, Millipore, Bedford, MA, USA).

Observation of the dissipative structures

Of the suspensions, 0.05 ml was dropped carefully and gently on a micro-cover glass (30×30 mm, thickness no. 1, 0.12 to 0.17 mm, Matsunami Glass, Kishiwada, Osaka) set in a temperature–humidity regulator (type KCL-2000, Tokyo Rikakikai, Tokyo). The box part of the sample room of the instrument is shown schematically in Fig. 1. Direct hit of the regulated air flow on the sample was prevented as possible. The cover glasses were used without further rinse. The contact angle for the pure water was 31±0.5° from the drop profiles of water on the cover glass. Extrapolation to the zero amount of water was made from the measurements at the several amount of water. A disposable serological pipet (1.0 ml, Corning Lab. Sci.) was used for the dropping the suspension on a cover glass. Observation of the macroscopic and microscopic drying patterns was made for the film formed after the suspension was dried up completely on a cover glass in the temperature–humidity regulator at 25, 40, or 80 °C in temperature and 40 or 80% in humidity. Sphere concentrations were 0.0001, 0.001, 0.01, and 0.1 in volume fraction.

Dissipative patterns were observed with a digital HD microscope (type VH-7000, Keyence, Osaka) and a laser 3D profile microscope (type VK-8500, Keyence). Close-up pictures were also taken on a Canon EOS 100QD camera with a macro-lens (EF 50 mm, f=2.5) and a life-size converter EF.

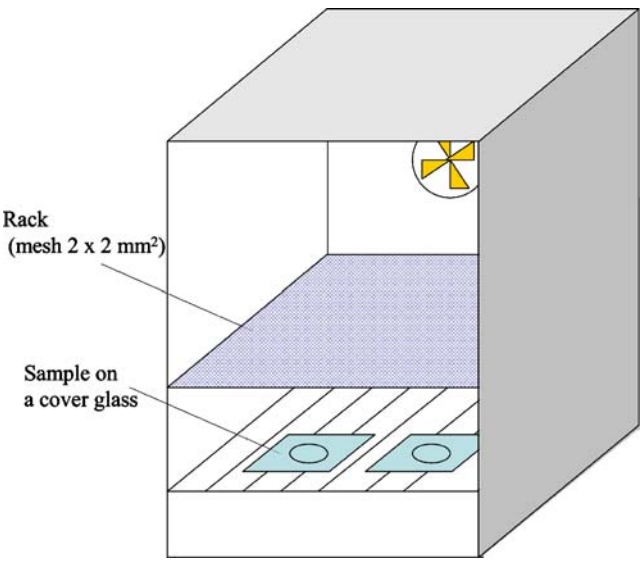

Fig. 1 Schematic picture of the sample room box of a temperature–humidity regulator, type KCL-2000. *Front of the box* is shielded with a door having a glass window, although the door is not shown in the figure

Results and discussion

Influences of temperature and humidity on the evaporation rate

The evaporation rate of water, R from a liquid surface to air, is proportional to the difference of the vapor pressures at the surface of the liquid (p_s) and the surrounding air (p), and given by Eq. 1.

$$R = KS(p_s - p), \tag{1}$$

where K is the coefficient and S the exposed surface area of the liquid on a cover glass. The overall evaporation rate coefficient, KS, contains all the information of the liquid shape on a cover glass, airflow pattern, and the heat transfer pattern during dryness between the liquid and the cell. At low solute concentrations, the vapor pressure of the liquid is close to that of water. At high solute concentrations, however, the pressure is reduced to lower values. Furthermore, it should be noted that the vapor pressure at the liquid surface, p_s, is further low in some extent, as the temperature at the liquid surface, T_s, is lowered by the evaporation of water. According to the principle of a psychrometer, the difference between the temperature of air and that at the liquid surface, $T-T_s$, is deeply correlated to the vapor pressure difference, p_s-p, and given by Eq. 2.

$$p_s - p = C(T - T_s) \tag{2}$$

Here, C is the constant being sensitive to the observation cell system. Equation 2 shows that the temperature (T_s) at the liquid surface linearly increases from a certain temperature lower than the T value as humidity (H) of the air increases from 0 to 100%. When H is 100%, T_s coincides with T.

From Eqs. 1, and 2, and 3 is derived easily.

$$R = KSC(T - T_s) \quad (3)$$

Equation 3 clearly shows that the convectional flow comes faster when temperature increases and/or humidity decreases through decreasing of T_s. In the present work, the experimental evaluation of R was not made, as the room space and the window of the temperature–humidity regulator was not large enough to analyze R values. However, Eqs. 1, and 2, and 3 are essentially important for the discussion of the role of temperature and humidity in the drying dissipative pattern. The values of p_s–p at 25 °C were estimated to be 1,550 and 360 Pa at H=40 and 80%, respectively, and those at 40 °C were 2670 Pa and 720 Pa, respectively. Thus, the magnitudes of the temperature lowering at the liquid surface at T=25 °C were estimated to be −2 and −1.5 °C at H=40 and 80%, respectively, and those at 40 °C were −5 and −2 °C, respectively.

Influences of temperature and humidity on the drying patterns, especially macroscopic broad rings

Figures 2, 3 and 4 show the drying dissipative patterns at temperatures (T) of 25, 40, and 80 °C, respectively. In each figures, sphere concentrations (ϕ) are 0.0001, 0.001, 0.01, and 0.1 in volume fraction, and relative humidities (H) are

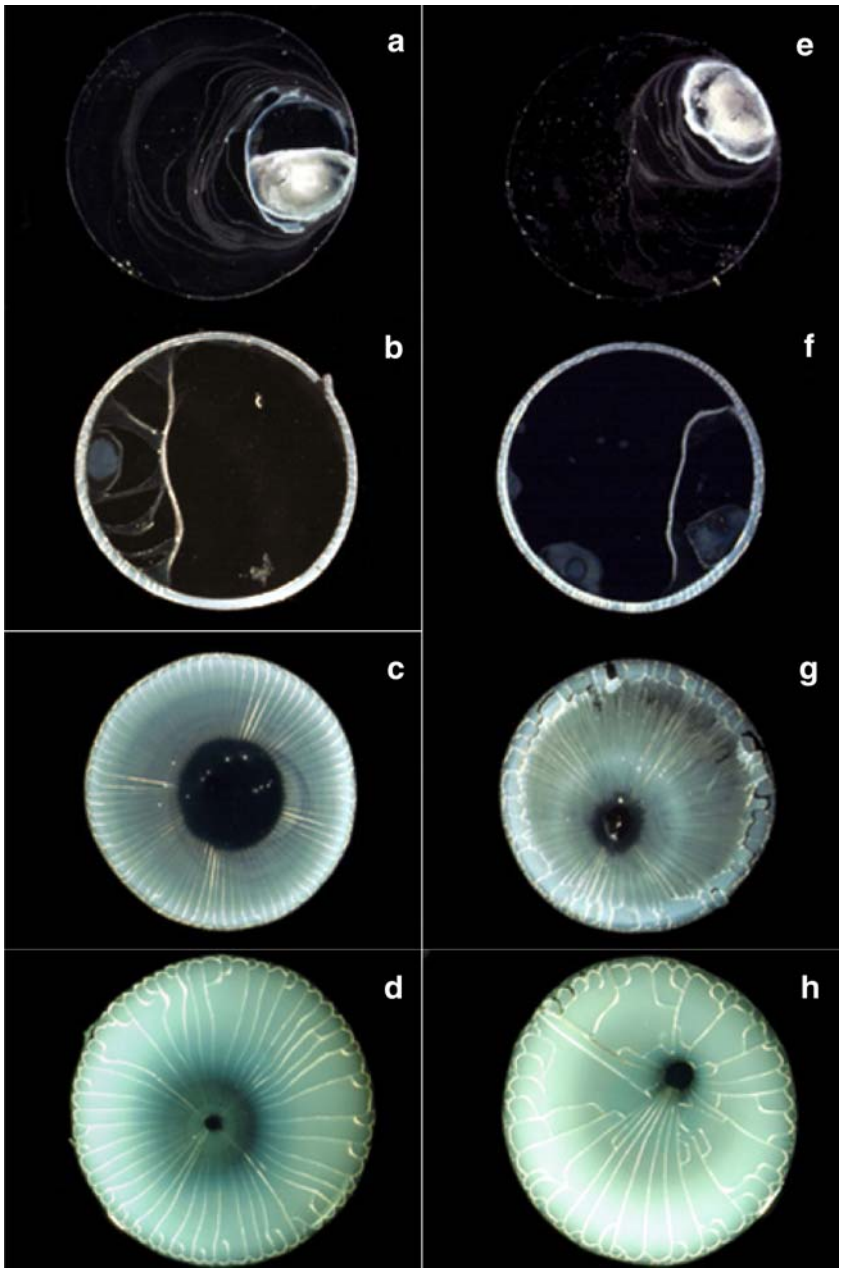

Fig. 2 Drying dissipative patterns of colloidal crystals of CS82 spheres on a cover glass at 25 °C. In water, 0.05 ml, **a** ϕ=0.0001, H=40%; **b** 0.001, 40%; **c** 0.01, 40%; **d** 0.1, 40%; **e** 0.0001, 80%; **f** 0.001, 80%; **g** 0.01, 80%; **h** 0.1, 80%; length of the bar is 1.0 mm

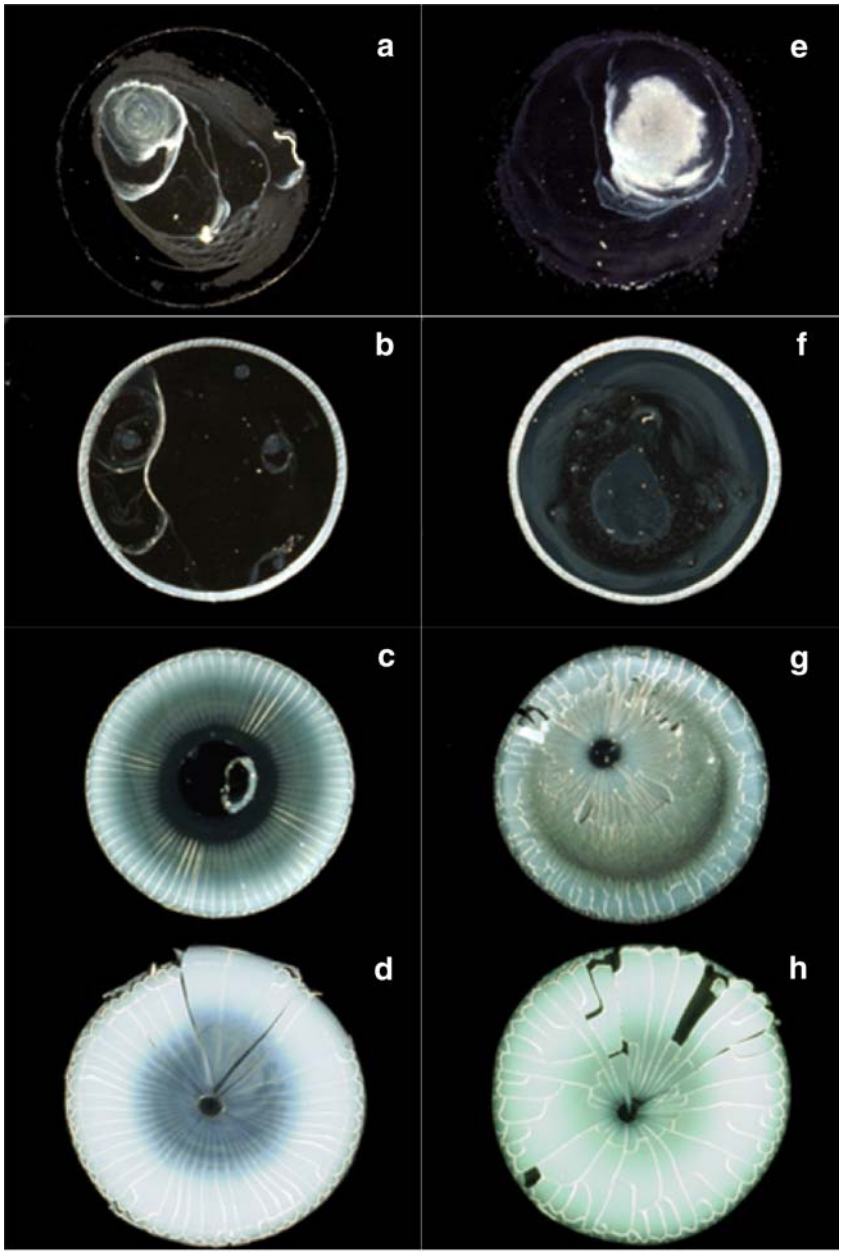

Fig. 3 Drying dissipative patterns of colloidal crystals of CS82 spheres on a cover glass at 40 °C. In water, 0.05 ml, **a** ϕ=0.0001, H=40%; **b** 0.001, 40%; **c** 0.01, 40%; **d** 0.1, 40%; **e** 0.0001, 80%; **f** 0.001, 80%; **g** 0.01, 80%; **h** 0.1, 80%; length of the bar is 1.0 mm

40 and 80%. Clearly, the broad ring, one of the typical macroscopic patterns, became sharp as T increased and/or H or ϕ decreased. The main cause for the broad ring formation is the convectional flow of water, as well as of colloidal spheres, in the direction from the center to the outside edges along the lower layers of the liquid. The convectional flow becomes faster when the evaporation rate of the solvent from the liquid surface increases, and the convectional flow of colloidal spheres increases when T increases and/or H decreases as is clearly shown in Eq. 3. Furthermore, the efficiency of the sphere accumulation toward outside edges, i.e., sharpness of the broad ring, by the convectional flow should be high when sphere concentration is low. Spoke-like cracks were also formed mainly in the region of the broad rings, and their number (N) increased as T and/or H decreased (see Table 2). These observations are consistent with the result that the broad rings become sharper with decreasing T or H. Furthermore, at high humidity, macroscopic patterns of both broad rings and the spoke-like cracks became more or less irregular in their patterns, and dried films were apt to break. It should be mentioned here that the dried films shown in Figs. 2, 3, and 4 at ϕ=0.01 and 0.1 were beautiful by their emitting iridescent colors. This supports strongly that all the sample suspensions are typical colloidal crystals, and the dried films are further keeping the crystal-like structures [44–48].

When sphere concentration is quite low, 0.0001 in volume fraction (see Figs 2a and e), most spheres moved

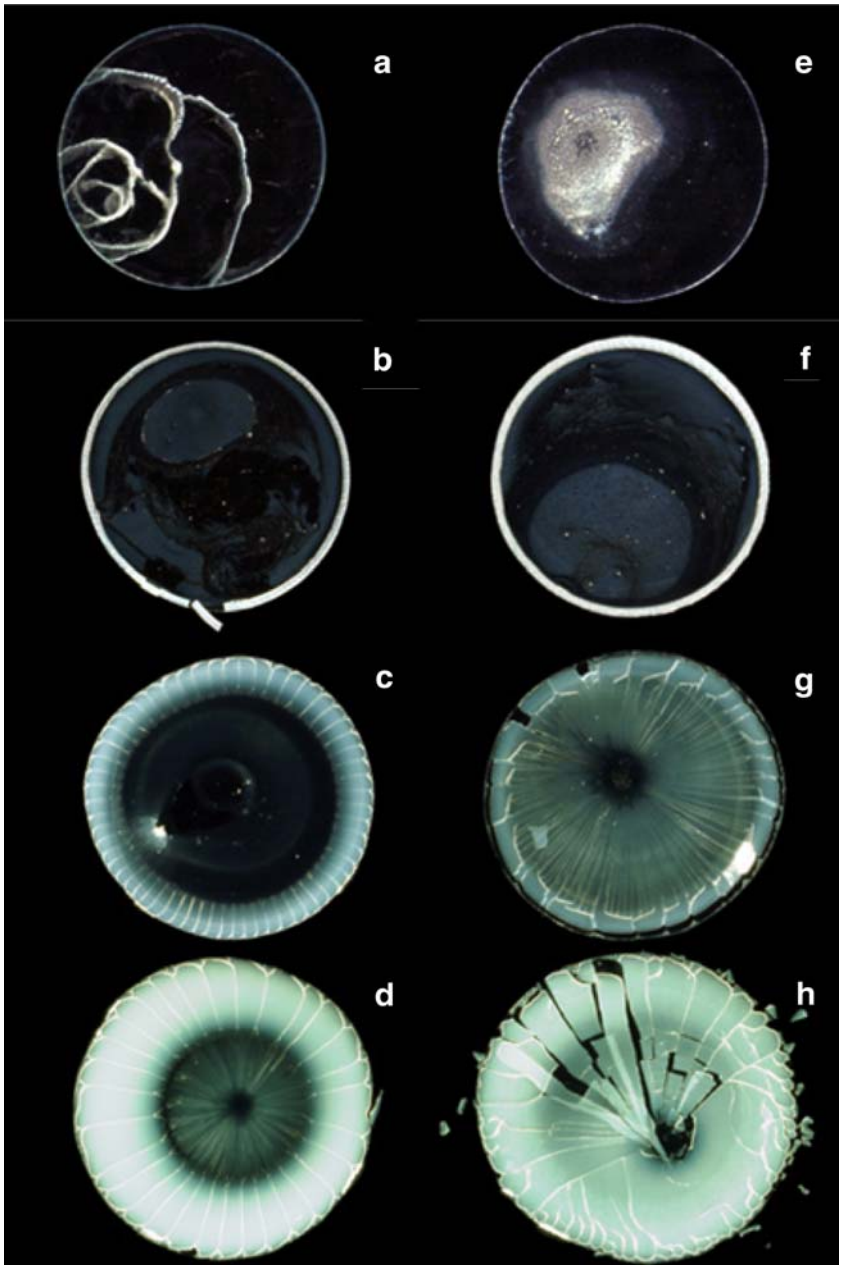

Fig. 4 Drying dissipative patterns of colloidal crystals of CS82 spheres on a cover glass at 80 °C. In water, 0.05 ml, **a** ϕ=0.0001, H=40%; **b** 0.001, 40%; **c** 0.01, 40%; **d** 0.1, 40%; **e** 0.0001, 80%; **f** 0.001, 80%; **g** 0.01, 80%; **h** 0.1, 80%; length of the bar is 1.0 mm

to the central area, and small broad ring pattern were formed at the central area. At ϕ=0.001, on the other hand, the dried patterns were not shrunk, and most spheres were accumulated at the outside edges, forming rather sharp broad rings as is shown in Figs. 2b and f. Interestingly, almost no humidity effect on the drying patterns was observed when sphere concentration is lower than 0.001 in volume fraction. When the sphere concentrations are high, ϕ=0.01 and 0.1, typical macroscopic broad-ring patterns were formed, and the rings were sharp at low H values (see Figs. 2c,d,g, and h). The patterns at T=40 °C (shown in Fig. 3) were quite similar to those at 25 °C (shown in Fig. 2). As temperature is raised, however, the sharpness of the broad rings and the decrease in the crack number were distinct from each other. We may understand these results because at the elevated temperatures, the convectional flow of the solvent and colloidal spheres should be fast compared with the flow at low temperature. At 80 °C, much more sharp broad rings and decrease in the number of the spoke-like cracks (N) were observed.

Influences of temperature and humidity on the drying patterns, especially macroscopic spoke-like cracks

The number (N) of the spoke-like cracks at the broad ring area is shown in Table 2 together with sphere concentration

Table 2 Number of spoke-like cracks (N) at the broad ring area as a function of sphere concentration (ϕ), temperature (T), and relative humidity (H)

T (°C)	H (%)	N	ϕ
0.01	25	40	74
0.01	25	80	64
0.01	40	40	70
0.01	40	80	58
0.01	80	40	59
0.01	80	80	29
0.1	25	40	38
0.1	25	80	20
0.1	40	40	41
0.1	40	80	30
0.1	80	40	30
0.1	80	80	20

(ϕ), T, and H data. Clearly, N decreased as ϕ, T, and H increased. Increase of ϕ and/or T is favor for the formation of thick broad rings resulting in a decrease in N, as the part of the thick broad ring is hard to be broken. It should be noted here that the spoke-like cracks are originated to the convectional spoke-like line pattern formed in the suspension state [1, 5]. The number of the spoke-like lines at the suspension state is considered to be much larger than that of the spoke-like cracks at the dried film. Actual number of the cracks in the dried film will be determined during the course of solidification, depending on the rigidity of the dried film, as the stresses and strains suffered on the dried film during the course of solidification must be vanished by the crack formation.

A clear-cut explanation for the observation of decrease in the spoke-like cracks at high values of H is not given yet

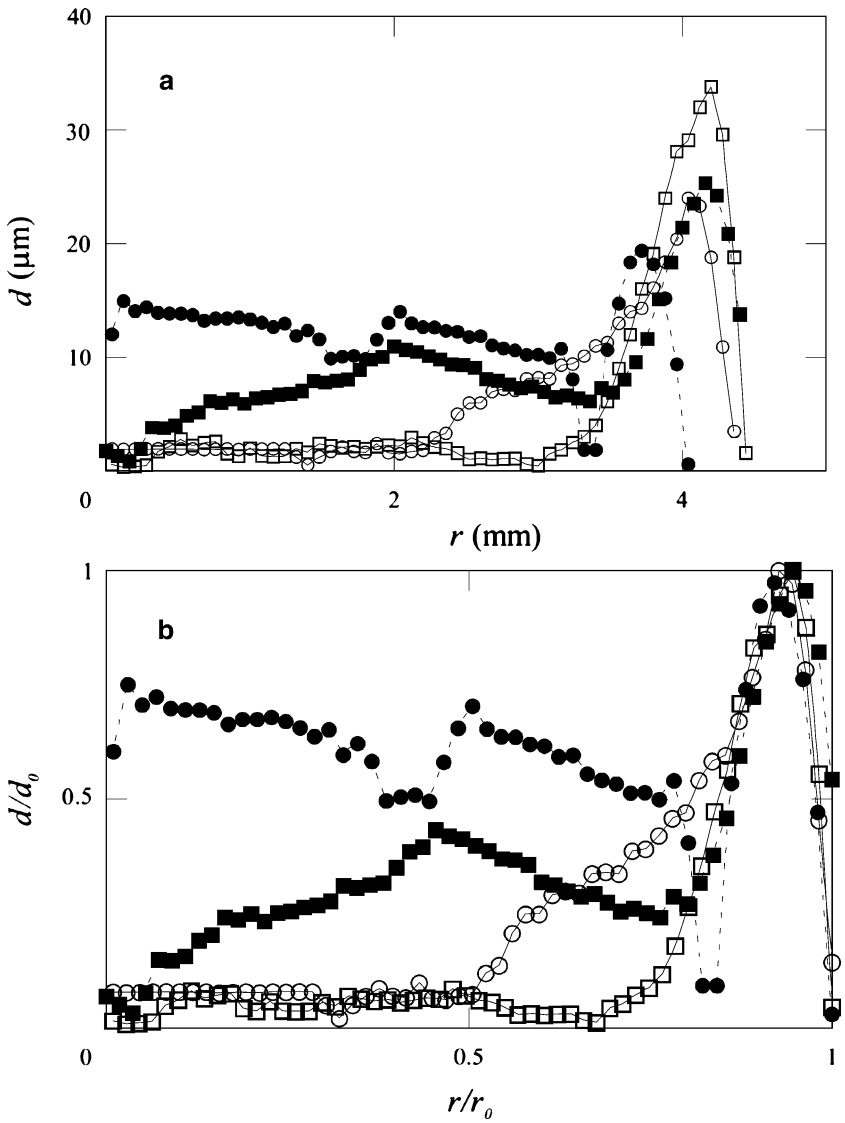

Fig. 5 **a** Thickness (d) profiles of dried films as a function of radius (r). In water, 0.05 ml, ϕ=0.01, *open circle* T=25 °C, H=40%; *open square* 80 °C, 40%; *filled circle* 25 °C, 80%; *filled square* 80 °C, 80%. **b** Thickness (d/d_o) profiles of dried films as a function of radius (r). In water, 0.05 ml, ϕ=0.01, *open circle* T=25 °C, H=40%; *open square* 80 °C, 40%; *filled circle* 25 °C, 80%; *filled square* 80 °C, 80%

at present. However, it is highly plausible that, at high humidity, the solidification rate by the convectional flow of solvent and the colloidal spheres is slow. Also plausible is that a part of the strains caused during the solidification processes will be canceled by the cooperative movement of the spheres.

Influences of temperature and humidity on the thickness profiles of the dried film

Thickness profiles of the dried films at $\phi = 0.01$ and 0.1 are shown in Figs. 5 and 6, respectively. Thickness of the films (d) is plotted as a function of the radial distance (r) from the film center of the corresponding film, the results of which are shown in Figs. 5a and 6a. Also shown in Figs. 5b and 6b are the normalized d/d_o vs r/r_o. Then, the normalization was made by the use of the maximum d and r values, i.e., d_o and r_o, respectively. As is clearly shown especially in Figs. 5b and 6b, sharp broad rings were formed when T was high and/or H was low, and then, the convectional flow was fast. Impressively, when T is 80 °C and H is 40%, most of the colloidal spheres moved toward outside edges, and the spheres at the central area were quite few compared with the spheres at the broad ring regions.

Summarizing the results of the present work, (1) the broad rings came sharp when T is high and/or H is low. (2) The number of spoke-like cracks around the broad ring regions decreased when T is high and/or H is high. Influences of temperature and humidity of air on the macroscopic drying patterns were quite substantial.

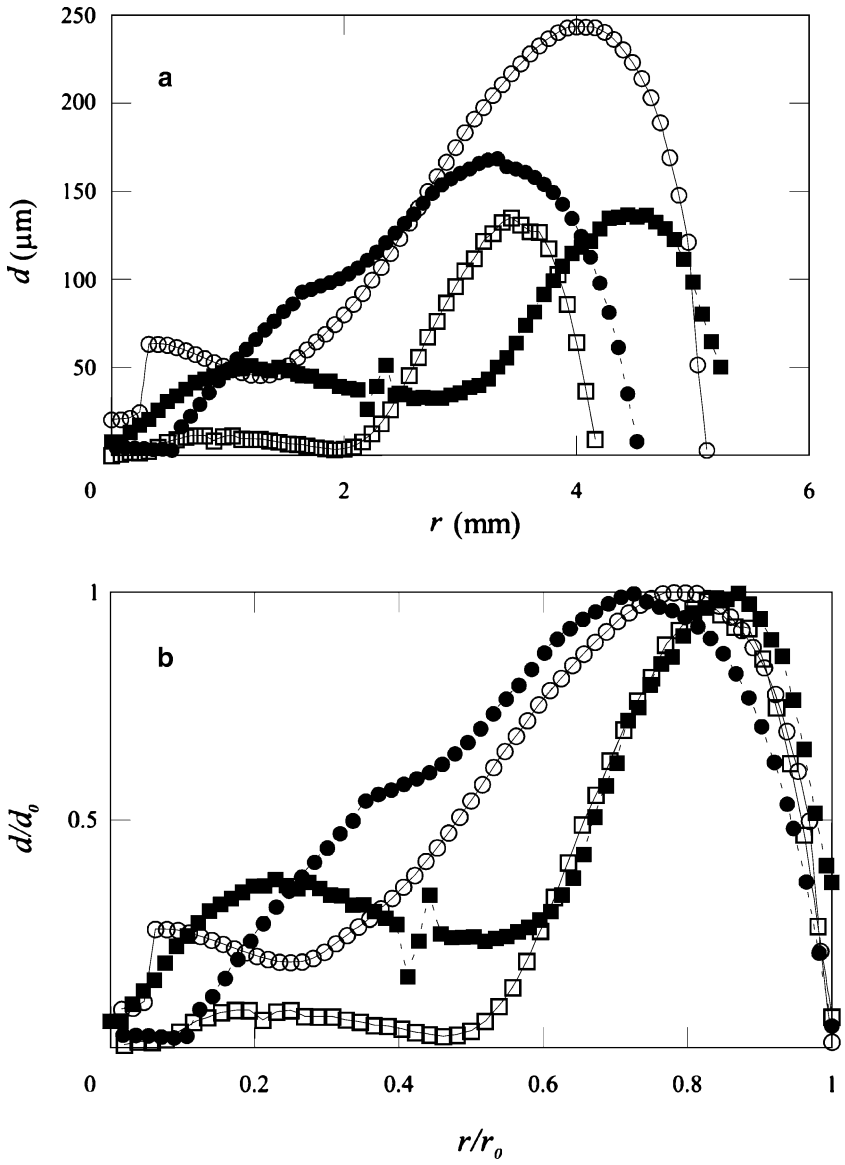

Fig. 6 **a** Thickness (d) profiles of dried films as a function of radius (r). In water, 0.05 ml, $\phi = 0.1$, *open circle* T=25 °C, H=40%; *open square* 80 °C, 40%; *filled circle* 25 °C, 80%; *filled square* 80 °C, 80%. **b** Thickness (d/d_o) profiles of dried films as a function of radius (r). In water, 0.05 ml, $\phi = 0.1$, *open circle* T=25 °C, H=40%; *open square* 80 °C, 40%; *filled circle* 25 °C, 80%; *filled square* 80 °C, 80%

Acknowledgment Financial support from the Ministry of Education, Culture, Sports, Science and Technology, Japan and Japan Society for the Promotion of Science are greatly acknowledged for Grants-in-Aid for Exploratory Research (17655046) and Scientific Research (B; 18350057 and 19350110-0001). The silica sphere sample, CS82, was a gift from Catalyst & Chemical Ind. (Tokyo), to whom the authors appreciate very much.

References

1. Okubo T, Okuda S, Kimura H (2002) Colloid Polym Sci 280:454
2. Okubo T, Kimura K, Kimura H (2002) Colloid Polym Sci 280:1001
3. Okubo T, Kanayama S, Ogawa H, Hibino M, Kimura K (2004) Colloid Polym Sci 282:230
4. Okubo T, Kanayama S, Kimura K (2004) Colloid Polym Sci 282:486
5. Okubo T, Kimura H, Kimura T, Hayakawa F, Shibata T, Kimura K (2005) Colloid Polym Sci 283:1
6. Okubo T, Yamada T, Kimura K, Tsuchida A (2005) Colloid Polym Sci 283:1007
7. Yamaguchi T, Kimura K, Tsuchida A, Okubo T Matsumoto M (2005) Colloid Polym Sci 283:1123
8. Kimura K, Kanayama S, Tsuchida A, Okubo T (2005) Colloid Polym Sci 283:898
9. Okubo T, Shinoda C, Kimura K, Tsuchida A (2005) Langmuir 21:9889
10. Okubo T, Yamada T, Kimura K, Tsuchida A (2006) Colloid Polym Sci 284:396
11. Okubo T (2006) Colloid Polym Sci 284:1395
12. Okubo T (2006) Colloid Polym Sci 284:1191
13. Okubo T (2006) Colloid Polym Sci 285:231
14. Okubo T (2006) Colloid Polym Sci 285:331
15. Okubo T, Itoh E, Tsuchida A, Kokufuta E (2006) Colloid Polmer Sci 285:339
16. Okubo T, Nozawa M, Tsuchida A (2007) Colloid Polym Sci 285:827
17. Okubo T, Kimura K, Tsuchida A (2007) Colloids Surf 56:201
18. Okubo T, Onoshima D, Tsuchida A (2007) Colloid Polym Sci 285:999
19. Okubo T, Okamoto J, Tsuchida A (2007) Colloid Polym Sci 285:967
20. Okubo T, Nakagawa N, Tsuchida A (2007) Colloid Polym Sci 285:1247
21. Okubo T, Yokota N, Tsuchida A (2007) Colloid Polym Sci 285:1257
22. Terada T, Yamamoto R, Watanabe T (1934) Proc Imp Acad (Tokyo) 10:10
23. Terada T, Yamamoto R, Watanabe T (1934) Sci Pap Inst Phys Chem Res Jpn 27:75
24. Terada T, Yamamoto R (1935) Proc Imp Acad (Tokyo) 11:214
25. Okubo T (2007) Colloid Polym Sci 285:1495
26. Ball P (1999) The self-made tapestry formation in nature. Oxford University Press, Oxford
27. Okubo T, Okamoto J, Tsuchida A Colloid Polym Sci (in press). DOI 10.1007/s00396-007-1778-6
28. Okubo T (2006) Molecular and colloidal electro-optics. In: Stoylov SP, Stoimenova MV (eds), p573, CRC Taylor & Francis, New York
29. Okubo T (2007) Nanoparticles: syntheses, passivation, stabilization and functionalization. In: Nagarajan (ed.), ACS Book, Am Chem Soc, Washington, DC (in press)
30. Vanderhoff JW, Bladford EB, Carrington WK (1973) J Polymer Sci Symp 41:155
31. Nicolis G, Prigogine I (1977) Self-organization in non-equilibrium systems. Wiley, New York
32. Cross MC, Hohenberg PC (1993) Rev Modern Phys 65:851
33. Adachi E, Dimitrov AS, Nagayama K (1995) Langmuir 11:1057
34. Ohara PC, Heath JR, Gelbart WM (1998) Langmuir 14:3418
35. Uno K, Hayashi K, Hayashi T, Ito K, Kitano H (1998) Colloid Polymer Sci 276:810
36. van Duffel B, Schoonheydt RA, Grim CPM, De Schryver FC (1999) Langmuir 15:957
37. Maenosono S, Dushkin CD, Saita S, Yamaguchi Y (1999) Langmuir 15:957
38. Nikoobakht B, Wang ZL, El-Sayed MA (2000) J Phys Chem 104:8635
39. Ge G, Brus L (2000) J Phys Chem 104:9573
40. Lin XM, Jaenger HM, Sorensen CM, Klabunde KJ (2001) J Phys Chem 105:3353
41. Ung T, Liz-Marzan LM, Mulvaney P (2001) J Phys Chem 105:3441
42. Haw MD, Gilli M, Poon WCK (2002) Langmuir 18:1626
43. Shimomura M, Sawadaishi T (2001) Curr Opin Colloid Interface Sci 6:11
44. Okubo T (1988) Acc Chem Res 21:281
45. Okubo T (1993) Prog Polym Sci 18:481
46. Okubo T (1994) Macro-ion characterization. From dilute solutions to complex fluids. In: Scxhmitz KS (ed) ACS Book. Am Chem Soc, Washington, DC, p 364
47. Okubo T (2002) Encyclopedia of surface and colloid science. In: Hubbard A (ed), p1300, Marcel Dekker
48. Okubo T (2005) Structural colors in biological systems. Principles and applications. In: Kinoshita S, Yoshioka S (eds) Osaka University Press, Osaka, Japan, p 267